International Journal of Applied Earth Observations and Geoinformation 117 (2023) 103131

Contents lists available at ScienceDirect

International Journal of Applied Earth Observations and Geoinformation

journal homepage: www.elsevier.com/locate/jag

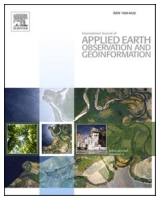

The potential of combining satellite and airborne remote sensing data for habitat classification and monitoring in forest landscapes

Anna Iglseder [a,*], Markus Immitzer [b], Alena Dostálová [a], Andreas Kasper [c], Norbert Pfeifer [a], Christoph Bauerhansl [d], Stefan Schöttl [d], Markus Hollaus [a]

[a] Department of Geodesy and Geoinformation, TU Wien, 1040 Vienna, Austria
[b] University of Natural Resources and Life Sciences, Vienna (BOKU), Institute of Geomatics, Peter-Jordan-Straße 82, 1190 Vienna, Austria
[c] Municipal Department 22 – Environmental Protection in Vienna (MA22), Dresdner Straße 45, 1200 Vienna, Austria
[d] Austrian Research Centre for Forests, Unit Remote Sensing, Seckendorff-Gudent-Weg 8, 1130 Vienna, Austria

ARTICLE INFO

Keywords:
Habitat Mapping
Natura 2000
Airborne Laser Scanning
Sentinel-1
Sentinel-2
Random Forest

ABSTRACT

Mapping and monitoring of habitats are requirements for protecting biodiversity. In this study, we investigated the benefit of combining airborne (laser scanning, image-based point clouds) and satellite-based (Sentinel 1 and 2) data for habitat classification. We used a two level random forest 10-fold leave-location-out cross-validation workflow to model Natura 2000 forest and grassland habitat types on a 10 m pixel scale at two study sites in Vienna, Austria. We showed that models using combined airborne and satellite-based remote sensing data perform significantly better for forests than airborne or satellite-based data alone. For frequently occurring classes, we reached class accuracies with F1-scores from 0.60 to 0.87. We identified clear difficulties of correctly assigning rare classes with model-based classification. Finally, we demonstrated the potential of the workflow to identify errors in reference data and point to the opportunities for integration in habitat mapping and monitoring.

1. Introduction

While the climate crisis has gained a lot of attention during the last years, a closely related crisis, the global loss of biodiversity, has just been brought to the fore recently (McElwee, 2021). During the last UN Climate Change Conference in Glasgow 2021 it was shown that these two challenges have to be addressed and solved simultaneously (COP26, 2021). For local measures of biodiversity protection, it is relevant to gain sufficient information about the current state and the development of small-scale, as well as large-scale green spaces. Comprehensive monitoring of green spaces reveals the state of climate-relevant, ecological, economic and social functions. Moreover, it points out to specific measures that can be taken to maintain, obtain or improve biodiversity.

To promote and harmonize such constant monitoring, relevant areas may be designated worthy of protection. One Europe-wide measure established the Natura 2000 network of areas of high biodiversity value (EUR-Lex, 2022). As of January 2021, 15.6 % of the area of Austria are classified as Natura 2000 regions with additional regions being already nominated (Umweltbundesamt, 2021). The Natura 2000 network aims to preserve, protect and improve the quality of the natural habitats and therefore promotes the maintenance of biodiversity and the necessity of human activities for preservation. As a part of the network, the member states define and prioritize distinct areas of conservation and should report on the implementation and the taken measures every-six years. (Council of the European Union, 1992). To describe and classify Natura 2000 areas, the scheme presented in the annex of the EU's Habitat's directive (HD) is used (Council of the European Union, 2006). The classification is based on characteristic plant species and communities as well as on abiotic features, e.g., occurrence area, bedrock, soil or geomorphological features.

To date, classification, mapping and monitoring mainly relies on expert-based fieldwork. This approach is labor-intensive and therefore difficult to be implemented in frequent monitoring and the required reporting. An opportunity to overcome this challenge is to include data-driven classification and monitoring of habitats. Therefore, it is necessary to find exhaustive data reflecting characteristic features of different

* Corresponding author.
E-mail addresses: anna.iglseder@geo.tuwien.ac.at (A. Iglseder), markus.immitzer@boku.ac.at (M. Immitzer), alena.dostalova@geo.tuwien.ac.at (A. Dostálová), andreas.kasper@wien.gv.at (A. Kasper), norbert.pfeifer@geo.tuwien.ac.at (N. Pfeifer), christoph.bauerhansl@bfw.gv.at (C. Bauerhansl), stefan.schoettl@bfw.gv.at (S. Schöttl), markus.hollaus@geo.tuwien.ac.at (M. Hollaus).

https://doi.org/10.1016/j.jag.2022.103131
Received 31 May 2022; Received in revised form 18 November 2022; Accepted 24 November 2022
Available online 12 January 2023

habitat types.

Remote sensing provides promising data for classification and monitoring of habitats. Morphological vegetation features derived from airborne laser scanning (ALS) point cloud data were shown to be useful as plant species predictors (Hollaus et al., 2009; Koenig and Höfle, 2016; Puliti et al., 2017). In addition, the potential of describing vegetation structure using ALS data was highlighted in several studies (Hollaus et al., 2006; Wagner et al., 2008; Lindberg et al., 2012; Leiterer et al., 2015; Coops et al., 2016; Guo et al., 2017). Apart from that, ALS data was previously shown to be powerful in deriving detailed terrain models for geomorphological features, especially in forested areas (Kraus and Pfeifer, 1998). ALS data seems therefore promising for habitat classification, but is usually acquired with a repetition rate of several years and therefore not appropriate for constant monitoring with high temporal resolution, e.g., on a yearly basis. In contrast to ALS data, satellite-based data (e.g. Copernicus' Sentinel data) shows the big advantage of a very high temporal resolution. Therefore, it is possible to derive phenological characteristics. Several studies show that this is beneficial for tree species classification (Dostálová et al., 2021, 2018; Immitzer et al., 2019; Lechner et al., 2022) and prediction of grassland or field crop diversity and condition (Fauvel et al., 2020; Ghassemi et al., 2022; Pfeil et al., 2020; Vreugdenhil et al., 2018; Vuolo et al., 2018). Additionally, monitoring could be conducted with a shorter repetition cycle.

Habitat mapping and monitoring with remotely sensed data was already shown to be promising in several published studies. Vegetation and terrain features derived from ALS data, partly combined with hyperspectral images and full waveform analysis, were used successfully for classifying and monitoring various Natura 2000 habitats (Bässler et al., 2011; Zlinszky et al., 2014, 2015; Alexander et al., 2015; Demarchi et al., 2020; Osińska-Skotak et al., 2021; Szporak-Wasilewska et al., 2021). Data from different satellite-based sensors like Sentinel 1 and 2 (S1 and S2) (Tarantino et al., 2021, Pesaresi et al., 2022, Le Dez et al., 2021), Landsat 8 (Pesaresi et al., 2020), MODIS (Sittaro et al., 2022) or Quickbird (Hernando et al., 2012) showed potential for classification and monitoring of various habitat groups like waterbodies, grassland, bogs, dunes or forests. Although numerous studies show the use of satellite data as well as ALS data and imagery, relatively few studies combine these data sources for habitat monitoring (Räsänen et al., 2014, Nijland et al., 2015, Plakman et al., 2020, Onojeghuo et al., 2021). In combined approaches, only few ALS-based features like canopy height model (CHM) or terrain features are included. Most of these studies base their analysis on pixel- or plot level. In contrast, the studies of Hernando et al. (2012), Plakman et al. (2020) and Räsänen et al. (2014) employed on object level-based approach with segmentation prior to the classification. The extensive number of studies on habitat mapping and monitoring using remotely sensed data reflects the broad relevance of the topic.

In this study, we combine a great variety of features from satellite-based remote sensing data of high temporal resolution (S1 and S2) and features from airborne remote sensing data with high geometric resolution such as ALS and image-based point cloud (IM) data. We explore the potential of combining different data sources to classify and monitor forest and grassland habitats of Natura 2000 areas on two study sites in Vienna, Austria. The aims of this study are (1) to investigate different combinations of remote sensing data for habitat classification of the study sites, (2) to create a comprehensive feature-derived habitat map and (3) to evaluate the results with regard to the potential and limits of remote sensing-based habitat mapping and monitoring.

We conduct these analyses with a random forest classification with recursive feature elimination using a 10-fold spatial leave location out cross validation (LLO-CV) approach, trained, tested and validated on the available Natura 2000 HD mapping of Vienna on a 10 m pixel size.

2. Data and methods

2.1. Habitats directive classification

In this study, we use habitat groups and types according to the HD classification (Council of the European Union, 2006; described in detail in European Commission, 2013). This classification scheme differentiates nine habitat groups with a total of 229 habitat types. The habitat types are defined by occurring plant species and species communities, as well as location parameters like soils or geomorphological characteristics and management characteristics (European Commission, 2013).

For this study, we select four habitat types of the group natural and semi-natural grassland formations (further referred to as grass or grassland) and seven forest types. The selected types are presented in Table 1. We refer to Council of the European Union (2006) and European Commission (2013) for a detailed ecological description of the different habitats. The habitat maps of the City of Vienna are available as open data (Stadt Wien - https://data.wien.gv.at, 2020). The most recent mapping was conducted in 2008 in expert-based field work.

2.2. Study sites

We chose the two study sites as representatives of the two main green area types in Vienna: hilly, mainly forested alpine foothills in western Vienna (A) and floodplains with river meadows and riparian forest vegetation along the Danube River (B).

Study site A (Vienna Woods) is located in the southwest of Vienna. The study site covers 28.3 km^2 and is situated in the geological unit of the "Flyschzone", and is therefore characterized by clay and sandstone. The hilly area is cut by three major valleys in the south, north and northeast. The altitude is between 214 m and 515 m above sea level (a.s.

Table 1
Habitat types investigated within the two study sites Vienna Woods (A) and Lobau (B), according to the Habitat's Directive (Council of the European Union, 2006). The sign * prior to the name indicates priority habitat types.

Habitat groups	Habitat type (NATURA 2000 Code)	Description
Natural and semi-natural grassland formations	6210	Semi-natural dry grasslands and scrubland facies on calcareous substrates (Festuco-Brometalia) (* important orchid sites)
	6240	* Sub-Pannonic steppic grasslands
	6410	Molinia meadows on calcareous, peaty or clayey-silt-laden soils (Molinion caeruleae)
	6510	Lowland hay meadows (Alopecuruspratensis, Sanguisorba officinalis)
Forests	9110	Luzulo-Fagetum beech forests
	9130	Asperulo-Fagetum beech forests
	9170	Galio-Carpinetum oak-hornbeam forests
	9180	* Tilio-Acerion forests of slopes, screes and ravines
	91E0	* Alluvial forests with Alnus glutinosa and Fraxinus excelsior (Alno-Padion, Alnion incanae, Salicion albae)
	91F0	Riparian mixed forests of Quercus robur, Ulmus laevis and Ulmus minor, Fraxinus excelsior or Fraxinus angustifolia, along the great rivers (Ulmenion minoris)
	91G0	*Pannonic woods with Quercus petraea and Carpinus betulus

l.). Forests, with the major occurring forest types of oak-hornbeam and beech forests, dominate the area. The meadows in between are mainly lowland hay meadows. The study site covers the Viennese recreation area “Lainzer Tiergarten”, is part of the “Biosphärenpark Wienerwald” and entirely classified as Natura 2000 nature protection area.

Study site B (Lobau) is part of the “Donau-Auen” National Park in the riparian forests along the Danube River in the southeast of Vienna. The 22.9 km^2 of study site B are mainly flat with indications of a former dominant and now partly regulated braided river system and a floodplain landscape. The mean altitude is 153 m a.s.l., stretching from 147 m to 163 m. The main vegetation is again forests, with a dominance of alluvial forests and riparian mixed forests.

Fig. 1 shows the habitat group and habitat type coverage for both study sites. We excluded 13.8 % of the area of study site A and 45.3 % of the area of study site B from further analysis, as shown in the habitat group pie charts. These areas were either not assigned to a habitat type during the initial mapping or excluded due to limited occurrence. The threshold for a habitat type to be included was set to a minimum of three independent locations of a minimum of 1 ha each within the study site. Furthermore, the different locations must be without a buffer of 1 km from each other to prevent spatial autocorrelation.

2.3. Remote sensing data

As input features for the classification, we use point clouds from ALS, and image-based point clouds from aerial photographs (IM) as well as data from S1 and S2. In the following sections, the data are described in more detail.

2.3.1. High resolution point cloud data

The ALS data covers the entire area of the City of Vienna and was collected between November 9th and November 24th 2015 under leaf-off conditions in eight flight campaigns. Two different sensors were used for the data acquisition: a Riegl LMS-Q680i and a Riegl LMS-Q560 (RIEGL Laser Measurement Systems, Horn, Austria). Both scanners provide full waveform data acquisition (RIEGL Laser Measurement Systems, 2012, 2010). The median point density for the whole city area is 27 echoes/m^2 for 97 % with up to 12 echoes per beam. A preliminary point cloud classification (ground, vegetation, buildings, high points, water bridges, others and errors) was available.

For deriving the IM point cloud, aerial photographs were used. These aerial photographs were acquired during summer 2018 under leaf-on conditions and cover the entire area of the City of Vienna. The camera used was an Ultracam Eagle Mark 2 from Vexcel. The ground sampling distance (pixel size on the ground) was at least 20 cm. The overlapping in flight direction was at least 80 %, the overlapping at right angles to flight direction at least 30 %. The IM point cloud was created using the software MatchT from Trimble (Trimble, 2022). In addition to the 3D coordinates, the points are attributed with information from the four used spectral channels (red, green, blue, colored near infrared).

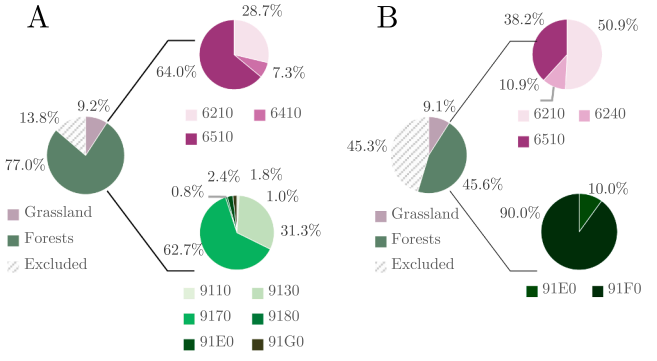

Fig. 1. The coverage of different habitat types of the two study sites A and B. The descriptions of the different classes are shown in Table 1. The excluded areas are not considered for the further classification.

2.3.2. Sentinel data

The Sentinel satellites are part of the European Commission’s and European Space Agency’s (ESA) Copernicus program for earth observation. The data is openly available.

S1 provides data from an active synthetic aperture radar (SAR) sensor. The used tiles are derived from S1 in C band at a pixel spacing of 10 m from the vegetation period of 2018. In detail, we use the Level 1B high resolution ground range detected (GRDH) and Level 1a single look complex (SLC) scenes acquired in the Interferometric Wide (IW) swath mode. The data from the relative orbits 22 (descending) and 146 (ascending) was extracted separately. The data was seasonally (February to March, June to August, October to November) and annually averaged.

S2 holds a passive sensor providing multispectral image data. For the study, we selected three cloud-free scenes from 2018. The scenes were acquired at different stages of the vegetation period on June 2nd, August 9th and September 28th 2018. For each scene, ten different bands (from 10 m to 20 m original resolution) were used for further feature extraction.

2.4. Feature extraction

We derived various features as raster layers for the model input. Therefore, we used the software packages OPALS (OPALS Development Team, 2022), GDAL (Rouault et al., 2022), SAGA (Conrad et al., 2015), QGIS (QGIS Development Team, 2022) and R (R Development Core Team, 2022).

The Sentinel features were party resampled and calculated at 10 m grid size, the features from ALS and IM point clouds at 1 m grid size. These 1 m grid size features were subsequently resampled to a 10 m grid. Therefore, statistical measures (mean, median, standard derivation) are derived. All features are transformed and reprojected to MGI / Austria GK East (EPSG 31256). An overview of the derived features is given in Table 2. In the following paragraphs of this chapter, we describe the features that might be unclear or unknown to the reader in more detail and give references to publications which show the exact calculations.

A digital terrain model (DTM), derived from the ALS point cloud, is the basis for the feature set of terrain features. Terrain features describe the absolute orientation as well as the relative position of a pixel in its surrounding. We split the aspect in sine (east–west exposition) and cosine (north–south exposition) to avoid the numerical challenges close to 0° / 360° north. The TPI measures the relative slope position of a pixel (De Reu et al., 2013), the TWI indicates potential runoff (Sørensen et al., 2006). We used the preliminary point cloud classification for the water surface distances in horizontal and vertical direction. The vertical distance to the closest water surface serves as a proxy for the groundwater level.

Gap fraction, FC and LAI of the ALS feature set are different measures for vegetation coverage. The gap fraction shows the proportion of pixels with a DSM < 0.02 m in a 10 m radius, the fractional cover is calculated as the share of first echoes higher than 1.5 m of all first echoes per m^2. The LAI is the fraction of leaf area to ground area and approximated by the share of first echo points to last and single echo points per m^2 (Morsdorf et al. 2006). The VCI, the understory height and the mean maximum echo number give information about the vegetation structure. The VCI describes the evenness of the point distribution within a voxel column (van Ewijk et al. 2011). Only points with higher than 0.2 m above ground are considered. The mean maximum echo serves as a proxy for vegetation density over the observed vegetation column. We calculated visibility features using the Solar Radiation and Annual Insolation Tool of SAGA (Conrad, 2018, 2010). We approximate the annual sums of potential radiation and insolation hours by calculating the values for a representative day per month. From the full waveform analysis, the echo width was extracted at terrain and surface level and

Table 2
Features derived from different remote sensing data. FM: February and March, JJA: June, July and August, ON: October and November. ∑ shows the number of derived features per feature set.

Feature set	Subgroups	Features	Aggregation and resampling	∑
Terrain features (TF)	Topographic features	Sine of aspect, cosine of aspect, slope [deg], topographic positioning index (TPI), topographic wetness index (TWI)	Mean, median, standard deviation from 1 m pixels	17
	Distance to water	Horizontal and vertical distance to water [m]	Mean from 1 m pixels	
ALS	Vegetation structure	Normalized digital surface model (nDSM) [m], height quantile 90 % [m], gap fraction, fractional cover (FC), understory height [m], leaf area index (LAI), vertical complexity index (VCI), maximum number of echoes per beam	Mean, median, standard deviation from 1 m pixels	45
	Visibility (from DSM - ALS)	Duration of insolation [h], diffuse, direct and total radiation [kWh/m^2]		
	Full-waveform analysis	Amplitude ratio surface/ground, pulse width surface [nm], pulse width terrain [nm]		
IM	Vegetation structure	nDSM [m]	Mean, median, standard deviation from 1 m pixels	30
	Visibility (from DSM - IM)	Duration of insolation [h], diffuse, direct and total radiation [kWh/m^2]		
	Spectral data	Blue, green, red, infrared, normalized difference vegetation index (NDVI)		
S1		Vertically polarized sent – vertically polarized received (VV) and vertically polarized sent – horizontally polarized received (VH) backscatter, cross ratio VH/VV, coherence	FM, JJA, ON, changes from FM to JJA and from JJA to ON, separate for each orbit	44
		Slope VV and VH, correlation VV and VH	Yearly, orbits combined	
S2	Spectral bands	B02, B03, B04, B05, B06, B07, B08, B8A, B11, B12	02.07.2018 (t1), 09.08.2018 (t2), 28.09.2018 (t3), changes from t1 to t2, changes from t2 to t3	165
	Vegetation indices	BAI, GCI, GEMI, GI, gNDVI, LCCI, NDRESSWIR, NDVI, NDVI2, reNDVI, REPA, RETVI, SAVI, SRBRE1, SRBRE2, SRBRE3, SRNIRB, SRNIRG, SRNIRR, SRNIRRE1, SRNIRRE2, SRNIRRE3, WBI – see Immitzer et al. (2019) for further details.		
Total number of features				301

the ratio between surface and ground amplitude was calculated. The echo width serves as a proxy for roughness, the amplitude as a radiometric property (Fieber et al., 2013).

From the IM point cloud, the nDSM and the visibility features are derived equally to the equivalent ALS features. The idea behind this approach is to test the interchangeability of ALS and IM data. Additionally, we used the spectral information of the IM point clouds, i.e., the spectral bands blue, green, red, near infrared (NIR) and the derived NDVI.

From S1-data, we extracted features sensitive to phenological characteristics of vegetation as well as canopy structures. Higher contributions of VH backscatter are typically seen as an indicator for volume scattering in vegetation canopies. Interferometric coherence was estimated between subsequent acquisitions with a temporal baseline of six days. This feature correlates the reflected phases of the same areas between six days, where low correlation (< 0.3) indicates dynamic surfaces like water or vegetation. The features slope and correlation are calculated for both VV and VH polarization annually. Slope describes the relation between radiation incidence angle and backscatter coefficient as the regression gradient, while correlation represents the corresponding correlation coefficient. These values give hints about vegetation types and densities. The sensitivity of the described features for vegetation monitoring was already shown in several studies (Bruggisser et al., 2021; Vreugdenhil et al., 2018). Dostálová et al. (2018) show the data processing in more detail.

From the S2 scenes, 23 vegetation indices were derived in addition to the original ten spectral bands. An extensive description of the used vegetation indices is shown by Immitzer et al. (2019). The changes between the different dates (both for S1 and S2 features) were calculated by subtracting the temporally latter from former feature values.

2.5. Model training, prediction and performance evaluation

We utilize the derived features as input for a classification based on a random forest model (Belgiu and Drăguţ, 2016; Breiman, 2001) with recursive feature elimination (RFE) using mean decrease in accuracy as described by Immitzer et al., (2012). We implemented the workflow in R (R Development Core Team, 2022) using the RandomForest package (Liaw and Wiener, 2002). The habitat mapping described in 2.1 serves as training as well as test data.

The workflow is split up into a two-step process as shown in Fig. 2. In a first step, the RFE evaluates all different feature combinations. Input features are ranked by importance and subsequently reduced until the best performing feature combination is selected. We limit the training sample to max. 2500 pixels per considered class to create a more balanced data set and exclude areas within a 10 m distance from class borders to limit boundary conditions.

In a second step, the optimal feature combination serves as input data for a 10-fold spatial LLO-CV setting. For this approach, we create the folds spatially and slice each study site in east–west direction into ten areas of equal size. One necessary condition for classes to be included is that every class considered is present within at least three different slices. We selected the 10-fold spatial LLO-CV approach to exclude the effects of spatial autocorrelation when applying the models on the test areas (as described by Meyer et al., 2018) and to get an independent model-based classification for the whole area of the study sites. For each fold of the LLO-CV, training pixels are selected randomly from the nine training folds. Again, we set the maximum number of pixels per class to 2500 and exclude 10 m distance from class borders. Using these pixels, we train a model and obtain the out-of-bag (OOB) error as a first measure of accuracy. For a detailed description of the OOB error, see Breiman (2001). With the trained model, we subsequently predict the whole area of the test fold. By changing the test fold, we can predict the whole study sites comprehensively with ten model training and prediction runs.

For the RFE as well as for the 10-fold spatial LLO-CV, we set the number of trees of the random forest to 500. The number of variables used for splitting *mtry* is set to the rounded down square root of the number of input variables.

We apply this two-step process first on the level of habitat groups to

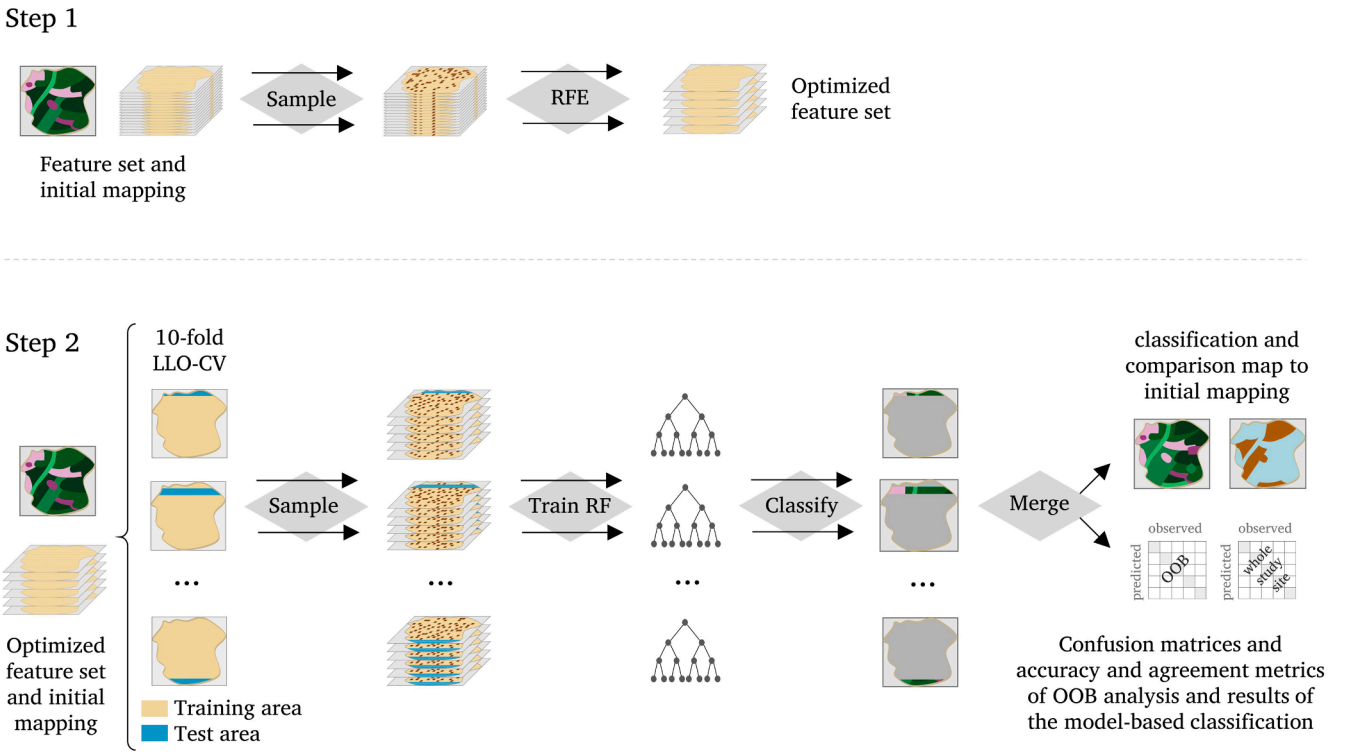

Fig. 2. Two-step classification workflow. Step 1. Optimizing input feature set by a recursive feature elimination (RFE) within random forest (RF) modelling (see Immitzer et al., 2012 for details). Step 2. Using the optimized feature set for training and applying of RF classifier in a 10-fold leave location out cross validation (LLO-CV) setup of the whole study area. For both steps, subsamples with max. 2 500 pixel per class are used. Confusion matrices and accuracy estimates are created both for out-of-bag (OOB) analysis during the model training and for the independent evaluation on the test sites. We run the workflow first for habitat groups (i.e., grassland, forest) and then, based on the group results, individually for different grassland and forest habitat types.

classify forest and grassland. In a consecutive step, we use this habitat group classification results as mask layers for the second-level classification of habitat types: the two-step process of RFE and 10-fold spatial LLO-CV is performed individually for grassland habitat types and forest habitat types. We compare and the final habitat group and type predictions to the reference data and validate the results by extracting confusion matrices and accuracy and agreement metrics (i.e., overall accuracy, kappa, user's (UA) and producer's accuracy (PA), F1-score). Additionally, we create maps to investigate spatial patterns of misclassifications.

We estimate the performance of all possible 31 different feature set combinations (FSCs) of the feature sets TF, ALS, IM, S1 and S2 to analyze the added values of different feature sets and investigate the combination of airborne and satellite-based remote sensing data for habitat classification. The described model training and classification is therefore conducted 31 times. We consider the OOB errors from the trained models as well as the overall accuracies to rank the performance of different FSCs. The OOB errors are averaged over the 10 folds of each FSC.

The 31 FSCs are grouped to ten single and 21 combined FSCs. Single FSCs include either a single feature set or combinations of either airborne only (TF, ALS, IM) or satellite-based only (S1, S2) feature sets. Combined FSCs include a combination of airborne and satellite-based feature sets. We calculate the median OOB error and the median overall classification error for each classification (habitat groups, forest types and grassland types) for single FSCs and combined FSCs separately and analyze the significance of the median differences, due to skewed distribution, with a Mann-Whitney-U-Test.

2.6. Evaluation of the results

We evaluate the output of the model both in desktop and fieldwork. We compare the maps classified by the model to a series of annual orthophotos to detect possible dynamics in vegetation. Additionally, we investigate chosen areas with differences between reference and classification results in the field.

3. Results

3.1. Investigate feature set combinations

Table 2 shows the results of the comparison of single and combined FSCs. The median OOB error is obtained from the ten LLO-CV models, the overall classification error from the comprehensive application of the trained models on the whole study sites. The FSCs include the features selected by the individual RFE. We considered both values for the habitat group classification and separately for habitat type classification of forests and grassland. For all OOB errors and classifications, combined FSCs outperform single FSCs in regards to classification accuracy. OOB and overall classification errors are lower for combined FSCs for all considered classifications, and, with one exception (overall classification error of grass, study site B), all differences are significant on a 5 % significance level. We can therefore state that combining airborne and satellite-based remote sensing data leads to better classification results than using airborne or satellite-based data only.

One additional interesting outcome is visible in Table 3: we observe great differences between the median OOB error values and the median overall classification errors. A detailed look to the results confirms the observed trends. We assume this might be a result of spatial autocorrelation of randomly selected training pixels for tree generating and OOB testing during the model training. As an additional factor, some classes are underrepresented in the model training, although training samples were at least balanced regarding to the order of magnitude.

Table 3
Performance analysis of different feature set combinations (FSCs) after recursive feature elimination (RFE). Groups shows the results of the first level classification (discriminate grass and forest), forest and grass refer to the second level classification of different grassland habitat types and forest habitat types. The p-value relates to the result of the Mann-Whitney U Test for rank sum differences (n = 31, 10 single and 21 combined FSCs).

		OOB error			overall classification error		
		median single	median combined	p-value	median single	median combined	p-value
study site A	groups	1.9 %	1.5 %	< 0.001	4.4 %	4.2 %	0.044
	forest	14.5 %	12.4 %	0.008	49.6 %	41.7 %	< 0.001
	grass	9.4 %	5.1 %	0.002	45.1 %	39.9 %	< 0.001
study site B	groups	2.4 %	2.0 %	0.003	9.4 %	8.8 %	0.003
	forest	15.2 %	9.7 %	0.003	30.8 %	26.7 %	0.007
	grass	9.1 %	2.7 %	0.001	30.8 %	29.5 %	0.125

Table 4
Results of the habitat group classification for study site A based on the FSC of all input feature sets. (UA. user's accuracy = precision, PA: producer's accuracy = recall).

study site A		observed habitat groups		sum (pred.)	UA
		grass	forest		
predicted habitat groups [pixels]	grass	26 165	7866	34 031	76.9 %
	forest	2481	218 577	221 058	98.9 %
	sum (obs.)	28 646	226 443	255 089	
	PA	91.3 %	96.5 %		
	F1-score	0.835	0.977		
					overall accuracy: 95.9 %, kappa: 0.81

Table 5
Results of the habitat group classification for study site B based on the FSC of all input feature sets. (UA: user's accuracy = precision, PA: producer's accuracy = recall).

study site B		observed habitat groups		sum (pred.)	UA
		grass	forest		
predicted habitat groups [pixels]	grass	21 358	9884	31 242	68.4 %
	forest	1900	101 876	103 776	98.2 %
	sum (obs.)	23 258	111 760	135 018	
	PA	91.8 %	91.2 %		
	F1-score	0.784	0.945		
					overall accuracy: 91.3 %, kappa: 0.73

3.2. Comprehensive classification results

In 3.1, we showed the benefit of combining airborne and satellite based remote sensing data. Therefore, we are limiting the presentation of our further results to the FSC including all input feature sets (TF, ALS, IM, S1, S2). The detailed results for all different FSCs are shown in the supplements (Table A1). The FSC including all input features does not perform best for all classifications, but the differences are negligible and result from the randomization during the recursive feature elimination and random forest model training. In average of all considered OOB and overall classification errors, this FSC shows the best results and therefore we can assume that the model is generally robust.

3.2.1. Habitat group classification

In the first level of classification, we investigate the discrimination of the two habitat groups forest and grassland. Table 4 and Table 5 show the results for study sites A and B. For both study sites, the overall classification accuracy is higher than 90 % and the kappa for both study sites show high agreement values (0.81 and 0.73). The kappa values have to be interpreted statistically carefully considering class prevalence (Foody, 2020).

With UA and PA, we consider additionally class-specific accuracy measures. The UA is a probability measure: it represents the chance of a randomly selected pixel of a predicted class showing the same class in the reference data. The PA shows the share of the correctly classified

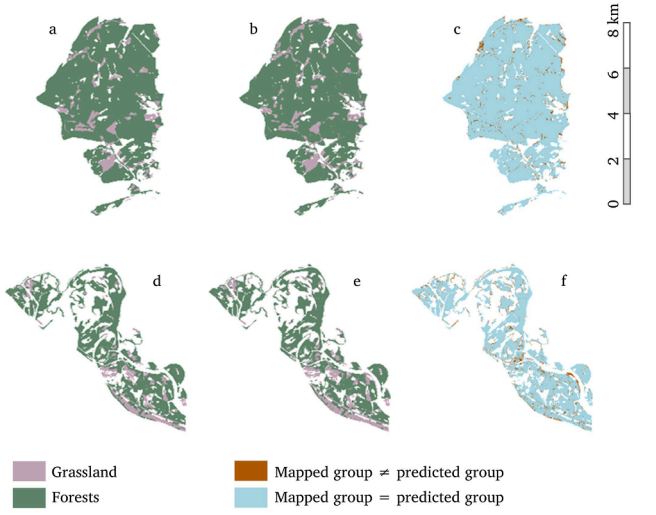

Fig. 3. Results of the habitat group classification. Sub-figures a-c refer to study site A, d-f to study site B. Sub-figures a and d show the reference data, b and e the predicted habitat groups. Sub-figures c and f indicate the differences of reference data and prediction.

reference pixels. The F1-score is the harmonic mean of PA and UA, represents a combined class-specific measure and is useful for comparing class performances of imbalanced data. For both study sites, we can see comparably lower UA values for grassland. Almost 1/4 (study site A) and 1/3 (study site B) of the pixels classified as grassland are mapped as forests in the reference data set. Comparing to the UA of forests, the opposite way of mapped forests classified as grasslands are neglectable with values lower than 2 % for both study sites. We can therefore assume an overestimation of grassland habitats for both study sites. Comparing the F1-scores, we see that the classifier performs better for forest habitats.

Fig. 3 shows the comparison of mapped habitat groups (reference data) and the maps of the model classification, including a directly comparing binary layer. We can see the spatial patterns of the confusion matrices results here. Most misclassified areas are one to three pixel-wide belts located at the border regions between grassland and forest habitats. Another source of misclassifications are small patches of grassland within forests: the classifier recognizes small clearings as grassland, while the reference data shows a generalized forest patch. Interestingly, single trees or small tree patches on grassland do not show up as small forest patches in grassland areas – the overestimation of grassland plays well here.

3.2.2. Habitat type classification

The second level of classification deals with habitat types within the forest and grassland habitat groups. We performed the two-step classification process independently for grassland and forest habitat types and combined the result in one confusion matrix and one map series per study site. Table 6 and Table 7 show the confusion matrices for study site A and B. For study site A, we get an overall accuracy of 63.0 % for nine habitat types and a kappa value of 0.43. For study site B, we reach a higher overall accuracy of 76.5 % and a kappa value of 0.54 for six habitat types. Parts of the overall classification errors are inherited from the first level of classification. The training data for the 10-fold spatial LLO-CV is depicted from the original mapping, but the prediction is made on the habitat group mask resulting from the first level classification described in 3.2.1.

The F1-scores reveal large differences in class accuracies. For study site A, the F1-scores range from 0.004 (class 9180) up to 0.719 (class 9170). The F1-scores of the habitat types of study site B show a smaller variety than the corresponding values of study site A ranging from 0.244 (class 6240) up to 0.869 (class 91F0). High F1-scores tend to occur more often for classes with a higher number of observed habitat pixels of a certain habitat type. Correlating the sum of observed habitat types and the F1-score for both study sites, a positive correlation of $p = 0.62$ is reached. The correlation of the sum of observed habitat types and the UA shows even higher correlation of $p = 0.72$. One explanation is that, although the training data was (partly) balanced, the greater variety of training pixels coming from a larger pool of independent habitat sites strengthens the classifier.

Fig. 4 shows the comparison of mapped habitat types (reference data) and the maps of the model classification with a binary layer comparing the two maps. In contrast to the habitat groups, there are obvious patterns of misclassification. Study site A shows large areas as well as small patches of differences between reference and classified maps more or less evenly distributed over the whole area. Study site B reveals hot spots of differences in the center region and in the north. A closer look on class level reveals some patterns: an observation we can make in both study sites is the overestimation of class 91E0 (Alluvial forests) close to water bodies. Furthermore, the maps reveal numerous differing pixels in habitat type border regions. While the reference data shows clear borders, the habitat type boundaries of the classified map are frayed.

3.3. Evaluation of the results

The evaluation of the results considers the mapped differences between reference data (i.e., mapped habitat groups and types) and model predictions (i.e., classified habitat groups and types) shown in Fig. 4, c and f. One challenge of the study that is important to be considered in this context is the different acquisition periods of remote sensing data for the model (2015 – 2018) and reference data (2008). We distinguish the differences between mapped and classified habitat groups and types between three different categories: 1) model classification errors, 2) initial mapping mistakes or inaccuracies 3) real changes of habitat groups or types. Following, we describe the evaluation of selected examples.

The focus of the desktop evaluation based on orthophoto inspection was on habitat groups. We can trace back some of the discrepancies of forest and grassland habitat groups with a closer look at the maps: one challenge arises with rasterizing the reference data that was originally provided in a vector. We can find extrapolations of up to half a pixel between two different classes and up to one pixel on external borders of the study site. Additionally, we could find ambiguous mapping strategies of forest/grassland borders (stem or canopy, with buffers in both direction) when comparing the vector data to orthophotos. These observations explain the misclassified belts described in 3.2.1. and can be seen as a combination of model classification errors and initial mapping inaccuracies. Other misclassification can be traced back to classification errors only: we found young forest stands misclassified as grassland. This might be a result of the low average height in the nDSM. Furthermore, we found explicit examples of initial mapping mistakes of habitat groups: areas, which can be clearly identified as forests in annual orthophoto series starting from 2006, are mapped as grassland in the

Table 6
Results of the habitat type classification for study site A based on the FSC of all input feature sets. (UA. user's accuracy = precision, PA. producer's accuracy = recall). Misclassifications with grey background are inherited from the first level classification (see Table 1 for class definitions).

study site A		observed habitat types [pixels]									sum (pred.)	UA
		6210	6410	6510	9110	9130	9170	9180	91E0	91G0		
predicted habitat types [pixels]	6210	3139	746	2714	22	1180	2539	26	199	222	10 787	29.1 %
	6410	228	259	99	0	54	171	0	12	6	829	31.2 %
	6510	3944	798	14 238	12	394	2067	10	699	253	22 415	63.5 %
	9110	5	0	10	18	1343	1727	83	74	29	3289	0.5 %
	9130	283	59	201	1221	44 585	30 384	782	236	520	78 271	57.0 %
	9170	609	112	580	520	19 961	93 951	905	632	2488	119 758	78.5 %
	9180	2	0	1	131	218	970	7	10	15	1354	0.5 %
	91E0	60	47	343	223	1400	5765	111	4584	673	13 206	34.7 %
	91G0	77	20	72	39	908	3826	33	159	46	5180	0.9 %
	sum (obs.)	8347	2041	18 258	2186	70 043	141 400	1957	6605	4252	255 089	
	PA	37.6 %	12.7 %	78.0 %	0.8 %	63.7 %	66.4 %	0.4 %	69.4 %	1.1 %		
	F1-score	0.328	0.180	0.700	0.007	0.601	0.719	0.004	0.463	0.010		
											overall accuracy: 63.0 %, kappa: 0.43	

Table 7
Results of the habitat type classification for study site A based on the FSC of all input feature sets. (UA: user's accuracy = precision, PA: producer's accuracy = recall). Misclassifications with grey background are inherited from the first level classification (see Table 1 for class definitions).

study site B		observed habitat types [pixels]					sum (pred.)	UA
		6210	6240	6510	91E0	91F0		
predicted habitat types [pixels]	6210	9454	1648	1244	1487	4914	18 747	50.4 %
	6240	905	648	48	306	767	2674	24.2 %
	6510	717	35	6659	628	1782	9821	67.8 %
	91E0	209	128	160	6142	12 514	19 153	32.1 %
	91F0	994	184	225	2780	80 440	84 623	95.1 %
	sum (obs.)	12 279	2643	8336	11 343	100 417	135 018	
	PA	77.0 %	24.5 %	79.9 %	54.1 %	80.1 %		
	F1-score	0.609	0.244	0.733	0.403	0.869		
							overall accuracy: 76.5 %, kappa: 0.54	

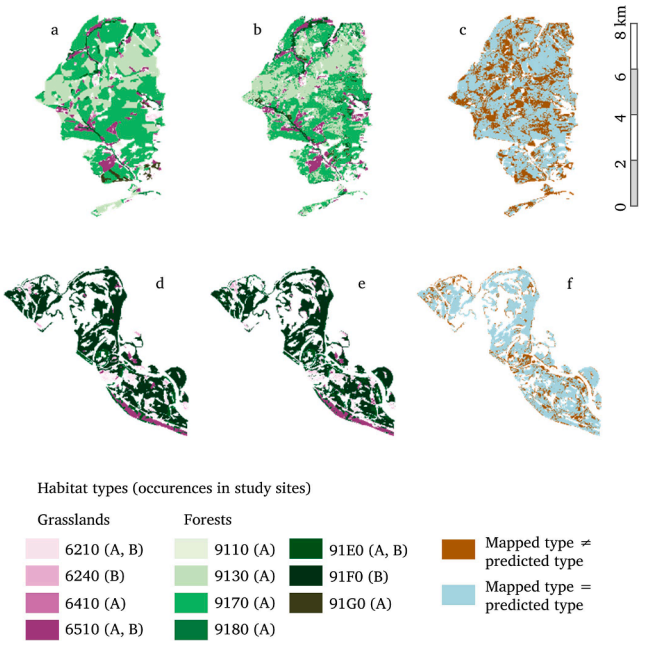

Fig. 4. Results of the habitat type classification. Sub-figures a-c refer to study site A, d-f to study site B. Sub-figures a and d show the reference data, b and e the predicted habitat types. Sub-figures c and f indicate the differences of reference data and prediction.

reference data.

We checked the habitat type maps in the field in October 2021 in both study sites for selected areas. Field evaluation revealed both areas of model classification errors and differences between the reference data and the situation in the field (differences of category 2 and 3). Dividing initial mapping errors and inaccuracies from real habitat changes turned out to be challenging for certain habitat types. We could identify areas of clear initial mapping errors, but we assume that some detected differences (for example the frayed habitat type boundaries) can be traced back to habitat shifts and habitat changes since the initial mapping of 2008.

A comprehensive and therefore quantifiable evaluation of the differences between mapped and classified habitat types and groups for the whole study sites was not possible in the scope of the study. Therefore, we cannot quantify the differences according to the categories of difference 1) – 3), but we assume the dominant shares are model classification errors.

4. Discussion

4.1. Investigation of different feature set combinations

We could clearly show that the combination of airborne and satellite-based remote sensing data is superior to airborne only as well as satellite-based only approaches for habitat classification in forest landscapes. Our findings are therefore in accordance with previous studies combining ALS and satellite-based data for tree species and forest classifications, like ALS and Landsat data for wildlife habitat classification (Nijland et al., 2015), ALS and S2 for tree species classification (Plakman et al., 2020) or ALS and QuickBird multispectral imagery for forest species classification (Ke et al., 2010). All studies highlighted the improvement in accuracy of the combined data approach. With our study, we can confirm the findings for habitat mapping and show that the differences are significant for forest habitat types and habitat groups.

For grasslands, we could show the significance only for one study site. This finding consists with study on grassland habitat discrimination using S2 time series: adding terrain information (DTM) to S2 data does not increase the overall accuracy, but F1-scores of single classes (Tarantino et al., 2021). The structure of grassland habitats tends to be less complex with a lower vegetation height. Therefore, we expect that ALS structure features have less explanatory power. Another impact is that simple structure changes like mowing can be detected by S1 coherence features (De Vroey et al., 2021) as well.

4.2. Out-of-bag error vs Overall classification error

For the ranking of the performance of different FSCs, we evaluated both OOB errors and overall classification errors and observed notable differences. For the chosen FSC of all feature sets, the OOB error and the overall classification error diverge by up to 6.9 percentage points for habitat groups, 24.5 percentage points for forest types and 27.8 percentage points for grassland types, where always the OOB error provides the lower values (i.e. more optimistic results). This outcome is contrary to previous studies (Immitzer et al., 2019; Lawrence et al., 2006; Vuolo et al., 2018; Zhong et al., 2014) stating that OOB errors are comparable to assessments based on a separate dataset for validation, presupposing that the reference data are well-distributed, representative and independent. In this context, we have to state that for our pixel-based approach, the training observations (pixels) in our models are to a large degree spatially dependent and therefore auto-correlated. This is especially true for small groups with only a few occurrences in the study site. We called for only three independent locations per class. Therefore, we expect auto-correlation within training data, although having a large number of training pixels (due to the defined prerequisites at least 2000 before boundary buffer elimination) per class. These spatial dependent training pixels can influence the results of bagging within the random forest model. This is negligible for ranking FSCs as done in 3.1, but for absolute accuracy assessment, we rely in our study on cross validation

rather than OOB errors. For the cross validation, we chose the 10-fold spatial LLO-CV as described by Meyer et al. (2018) to avoid spatial overfitting and make the overall accuracy robust. We propose further to consider this.

4.3. Classification accuracy

The overall accuracy of our model-based classification reaches 63.0 % for nine habitat types of study site A (six forest, three grassland types) and 76.5 % for five habitat types of study site B (two forest, three grassland types). Comparing the results directly to other studies on habitat classification is challenging, as input data, considered habitat types as well as study designs and scale vary. Nevertheless, the results are in line with similar studies on classification of HD habitat types. Bässler et al. (2011) achieve overall accuracies of 68.8 % and 72.6 % for four forest habitat types using ALS data. Demarchi et al. (2020) reach overall accuracies between 65.2 % and 77.4 % for three grassland habitat types with hyperspectral airborne images and ALS data, Zlinszky et al. (2014) show an overall accuracy of 68 % for 10 grassland classes and 75 % for five grassland classes using ALS data. Pesaresi et al. (2022) use S2 time series, topography and lithology as input for classifying eleven habitat types of different groups and reach an overall accuracy of 85.6 %. Räsänen et al. (2014) based their habitat classification on a different classification scheme and reached an overall accuracy of 79.1 % for 28 habitat types in a boreal forest landscape using high resolution satellite imagery, CHM and DTM.

We found that imbalanced class occurrences in the overall data have negative effects on class-specific accuracies for underrepresented classes. This is shown by comparably very low F1-scores for rare habitat types. These results reflect those of other studies (Immitzer et al., 2019; Sheeren et al., 2016). We showed that balancing training samples does not efficiently counteract the issue, as the individual observation (in our case pixels) are (spatially) dependent. This points to the importance of (at least group wise) independent training observations, not only independence between training and test data. Our minimum number of three independent locations of a minimum size of 1 ha (equals 1 000 observed pixels per location) turned out to be too little for a sound classification of the rare habitat types. One approach would be to buffer pixels within the training areas to avoid at least direct neighboring pixels. Therefore, it has to be discussed, what buffer on what scale guarantees pixels to be independent. Small classes are thus further reduced in size.

In 3.3 we addressed the challenges of different acquisition dates between reference data and model input data. We identified inaccuracies and errors of different sources in the reference data; therefore, accuracy estimates require a careful interpretation.

4.4. Evaluation of the results and usability for operational mapping and monitoring

Fig. 1 shows the share of the study site areas we used for our study: 13.8 % of study site A and 45.3 % of study site B were excluded from further analysis. These areas were either not assigned to a distinct class in the reference data or belong to rare classes and therefore offer too little data to train the model. The class accuracy results revealed that, from the model's perspective, even more classes should be excluded due to infrequent occurrence. Within the classification, we reduced the influence of spatial autocorrelation with the spatial partitioning of training and testing data. Nevertheless, training and testing area are still within the same landscape element, therefore the model accuracies only account for similar regions. We note that satisfactory area-wide habitat classification, including rare habitat types, cannot be achieved with our proposed approach.

The conditions described in the paragraph above make a discussion of the general usability of model-based habitat classification in operational use necessary. Despite all the limiting factors, we could reach good results for frequently occurring classes. All classes with more than 12 000 pixels in the study site reached F1-scores greater than 0.6. Hence, the trained models can at least support initial classification of regions similar to the investigated study sites. The models can reveal areas of common habitats and indicate areas with need for expert-based classification. For this, it can be helpful to show classification probabilities rather than an absolute assignment of a pixel to one class and apply the classification on homogeneous segments rather than pixels. Additionally, we showed that the model-based classification could assist in monitoring and evaluation of reference data. We could reveal initial mapping mistakes and indications of habitat shifts and changes. For monitoring, we can again state that our tested model can support expert-based fieldwork by pointing out areas worth investigating.

4.5. Limitations

The pixel-based approach of this study sets the minimum mapping unit of habitat types to squares of 100 m^2. We chose this approach in line with other studies working on habitat classification described in Chapter 1 Introduction. The benefits are the possibility for a straightforward classification without the need to define further homogeneity criteria or area sizes for mapping units. We identified the challenges and limits related to this approach clearly in this study, i.e., inaccuracies at boarder regions and scattered patterns. Another challenge of the pixel-based approach is the fusion of different data sources at different resolutions to a common grid. This leads to resample effects, especially as the raw data is initially provided in different coordinate reference systems. The results of the pixel-based approach could possibly be improved by morphological operations or label smoothing on the final maps to reduce salt-and-pepper effects (Li et al., 2019; Schindler, 2012). A different possibility would be the delineation of homogeneous segments prior to classification to use an object-based approach (Hernando et al., 2012; Räsänen et al., 2014). The challenge of this approach is to identify measures of homogeneity for object segmentation in the context of habitats, which are characterized by high biodiversity value.

The presented classification performs best on frequently occurring habitat types. Therefore, a clear limitation we state is the classification accuracy for habitat types with limited occurrence in the training data. Very rare types within the study sites were excluded prior to the model training and are therefore not considered at all in this study. As the monitoring of rare habitats is often of high interest, this is a clear drawback of the proposed approach. Considerations to address these limitations are to include classification probabilities to the mapping. By using class probabilities rather than assigning distinct classes to the pixels, rare habitats could probably be still be included in the model and classification uncertainties can be revealed.

A clear limitation of our presented approach is the fact, that the model is trained on very local conditions. Therefore, we only expect it to be useful to classify habitats in neighboring areas with similar topographic, hydrological and structural conditions. The support for local applications is anyway still valuable. For a more generalized and larger-scale mapping and monitoring of biodiversity we refer to the possibility of remote sensing data to estimate essential biodiversity variables (Skidmore et al., 2021).

5. Conclusion

In this study, we could show the benefit of combining airborne and satellite-based remote sensing data for habitat classification. We could show the significance of the combination of the data sources for habitat groups and forest habitat types. The high temporal resolution of Sentinel data provides information about dynamics, the high geometric resolution of airborne data gives insight in vegetation structure and topographic and spectral information on a smaller scale. Both information is useful and complementary for characterizing habitats.

We combined all feature sets from Sentinel-1 (S1), Sentinel-2 (S2), airborne laser scanning (ALS) and image-based point cloud (IM) data to

train a random forest model and predict the overall study sites using a 10-fold spatial leave-location-out cross validation (LLO-CV). With the presented workflow, we derived confusion matrices of different habitat types as well as habitat maps. We achieved overall accuracies of 63 % to 76.5 % for up to nine different habitat types per study site and class accuracies with F1-scores from 0.60 to 0.87 for frequently occurring forest and grassland habitat types. Additionally, we showed the capability of model-based classification maps to identify initial mapping errors in reference data and to monitor habitat distribution. In summary, we can state that habitat classification by trained models on pixel scale has a great potential to support expert-based habitat mapping and monitoring in forest landscapes.

CRediT authorship contribution statement

Anna Iglseder: Conceptualization, Methodology, Validation, Formal analysis, Investigation, Data curation, Writing – original draft, Visualization. **Markus Immitzer:** Methodology, Software, Formal analysis, Writing – review & editing. **Alena Dostálová:** Formal analysis. **Andreas Kasper:** Resources, Validation. **Norbert Pfeifer:** Writing – review & editing, Supervision. **Christoph Bauerhansl:** Resources. **Stefan Schöttl:** Resources. **Markus Hollaus:** Conceptualization, Methodology, Software, Writing – review & editing, Supervision, Project administration, Funding acquisition.

Declaration of Competing Interest

The authors declare that they have no known competing financial interests or personal relationships that could have appeared to influence the work reported in this paper.

Data availability

Data will be made available on request.

Acknowledgements

The ALS data are provided by the municipality of Vienna. The IM data are provided by the Austrian Research Centre for Forests. Sentinel-1 data were extracted from the Austrian Data Cube (ACube) operated by EODC and supported by the ACube partners and processed in the framework of the FFG Austrian Space Applications Programme ASAP 14 “Austrian Data Cube” project (grant agreement number 865999). The ALS and Sentinel-2 data processing and classification work was founded by the FFG Austrian Space Applications Programme ASAP 15 “Anwendungsmöglichkeiten von Sentinel-Daten für ein Monitoring im Umwelt- und Naturschutz in Städten am Beispiel Wien, SeMoNa22” (grant agreement number 881400). The authors acknowledge TU Wien Bibliothek for financial support through its Open Access Funding Programme.

Appendix A. Supplementary material

Supplementary data to this article can be found online at https://doi.org/10.1016/j.jag.2022.103131.

References

Alexander, C., Deák, B., Kania, A., Mücke, W., Heilmeier, H., 2015. Classification of vegetation in an open landscape using full-waveform airborne laser scanner data. Int. J. Appl. Earth Obs. Geoinformation 41, 76–87. https://doi.org/10.1016/j.jag.2015.04.014.

Bässler, C., Stadler, J., Müller, J., Förster, B., Göttlein, A., Brandl, R., 2011. LiDAR as a rapid tool to predict forest habitat types in Natura 2000 networks. Biodivers. Conserv. 20, 465–481. https://doi.org/10.1007/s10531-010-9959-x.

Belgiu, M., Drăguţ, L., 2016. Random forest in remote sensing: A review of applications and future directions. ISPRS J. Photogramm. Remote Sens. 114, 24–31. https://doi.org/10.1016/j.isprsjprs.2016.01.011.

Breiman, L., 2001. Random Forests. Mach. Learn. 45, 5–32. https://doi.org/10.1023/A:1010933404324.

Bruggisser, M., Dorigo, W., Dostálová, A., Hollaus, M., Navacchi, C., Schlaffer, S., Pfeifer, N., 2021. Potential of Sentinel-1 C-Band Time Series to Derive Structural Parameters of Temperate Deciduous Forests. Remote Sens. 13, 798. https://doi.org/10.3390/rs13040798.

European Commission, 2013. Interpretation Manual of European Union Habitats, version EUR 28 [WWW Document]. URL https://eunis.eea.europa.eu/references/2435 (accessed 28.4.22).

Conrad, O., Bechtel, B., Bock, M., Dietrich, H., Fischer, E., Gerlitz, L., Wehberg, J., Wichmann, V., Böhner, J., 2015. System for Automated Geoscientific Analyses (SAGA) v. 2.1.4. Geosci. Model Dev. 8, 1991–2007. https://doi.org/10.5194/gmd-8-1991-2015.

Conrad, O., 2010. Tool Potential Incoming Solar Radiation / SAGA-GIS Tool Library Documentation (v6.4.0) [WWW Document]. URL https://saga-gis.sourceforge.io/saga_tool_doc/6.4.0/ta_lighting_2.html (accessed 18.5.22).

Conrad, O., 2018. Tool Potential Annual Insolation / SAGA-GIS Tool Library Documentation (v7.6.1) [WWW Document]. URL https://saga-gis.sourceforge.io/saga_tool_doc/7.6.1/ta_lighting_7.html (accessed 18.5.22).

Coops, N.C., Tompaski, P., Nijland, W., Rickbeil, G.J.M., Nielsen, S.E., Bater, C.W., Stadt, J.J., 2016. A forest structure habitat index based on airborne laser scanning data. Ecol. Indic. 67, 346–357. https://doi.org/10.1016/j.ecolind.2016.02.057.

COP26, 2021. Protecting and restoring nature for the benefit of people and climate. [WWW Document]. UN Clim. Change Conf. COP26 SEC – Glasg. 2021. URL https://ukcop26.org/nature/ (accessed 7.4.22).

Council of the European Union, 2006. Council Directive 2006/105/EC of 20 November 2006 adapting Directives 73/239/EEC, 74/557/EEC and 2002/83/EC in the field of environment, by reason of the accession of Bulgaria and Romania, OJ L.

De Reu, J., Bourgeois, J., Bats, M., Zwertvaegher, A., Gelorini, V., De Smedt, P., Chu, W., Antrop, M., De Maeyer, P., Finke, P., Van Meirvenne, M., Verniers, J., Crombé, P., 2013. Application of the topographic position index to heterogeneous landscapes. Geomorphology 186, 39–49. https://doi.org/10.1016/j.geomorph.2012.12.015.

De Vroey, M., Radoux, J., Defourny, P., 2021. Grassland Mowing Detection Using Sentinel-1 Time Series: Potential and Limitations. Remote Sens. 13, 348. https://doi.org/10.3390/rs13030348.

Demarchi, L., Kania, A., Ciężkowski, W., Piórkowski, H., Oświecimska-Piasko, Z., Chormański, J., 2020. Recursive Feature Elimination and Random Forest Classification of Natura 2000 Grasslands in Lowland River Valleys of Poland Based on Airborne Hyperspectral and LiDAR Data Fusion. Remote Sens. 12, 1842. https://doi.org/10.3390/rs12111842.

Dostálová, A., Wagner, W., Milenković, M., Hollaus, M., 2018. Annual seasonality in Sentinel-1 signal for forest mapping and forest type classification. Int. J. Remote Sens. 39, 7738–7760. https://doi.org/10.1080/01431161.2018.1479788.

Dostálová, A., Lang, M., Ivanovs, J., Waser, L.T., Wagner, W., 2021. European Wide Forest Classification Based on Sentinel-1 Data. Remote Sens. 13, 337. https://doi.org/10.3390/rs13030337.

EUR-Lex, 2022. EUR-Lex - Natura 2000 [WWW Document]. URL https://eur-lex.europa.eu/EN/legal-content/glossary/natura-2000.html (accessed 26.4.22).

Fauvel, M., Lopes, M., Dubo, T., Rivers-Moore, J., Frison, P.-L., Gross, N., Ouin, A., 2020. Prediction of plant diversity in grasslands using Sentinel-1 and -2 satellite image time series. Remote Sens. Environ. 237, 111536 https://doi.org/10.1016/j.rse.2019.111536.

Fieber, K.D., Davenport, I.J., Ferryman, J.M., Gurney, R.J., Walker, J.P., Hacker, J.M., 2013. Analysis of full-waveform LiDAR data for classification of an orange orchard scene. ISPRS J. Photogramm. Remote Sens. 82, 63–82. https://doi.org/10.1016/j.isprsjprs.2013.05.002.

Council of the European Union, 1992. Council Directive 92/43/EEC of 21 May 1992 on the conservation of natural habitats and of wild fauna and flora, OJ L.

Foody, G.M., 2020. Explaining the unsuitability of the kappa coefficient in the assessment and comparison of the accuracy of thematic maps obtained by image classification. Remote Sens. Environ. 239, 111630 https://doi.org/10.1016/j.rse.2019.111630.

Ghassemi, B., Dujakovic, A., Żółtak, M., Immitzer, M., Atzberger, C., Vuolo, F., 2022. Designing a European-Wide Crop Type Mapping Approach Based on Machine Learning Algorithms Using LUCAS Field Survey and Sentinel-2 Data. Remote Sens. 14, 541. https://doi.org/10.3390/rs14030541.

Guo, X., Coops, N.C., Tompalski, P., Nielsen, S.E., Bater, C.W., John Stadt, J., 2017. Regional mapping of vegetation structure for biodiversity monitoring using airborne lidar data. Ecol. Inform. 38, 50–61. https://doi.org/10.1016/j.ecoinf.2017.01.005.

Hernando, A., Arroyo, L.A., Velázquez, J., Tejera, R., 2012. Objects-based Image Analysis for Mapping Natura 2000 Habitats to Improve Forest Management. Photogramm. Eng. Remote Sens. 78, 991–999. https://doi.org/10.14358/PERS.78.9.991.

Hollaus, M., Mücke, W., Höfle, B., Dorigo, W., Pfeifer, N., Wagner, W., Bauerhansl, C., Regner, B., 2009. Tree species classification based on full-waveform airborne laser scanning data. Presented at the Silvilaser 2009, College Station, Texas, USA, p. 10.

Hollaus, M., Wagner, W., Eberhöfer, C., Karel, W., 2006. Accuracy of large-scale canopy heights derived from LiDAR data under operational constraints in a complex alpine environment. ISPRS J. Photogramm. Remote Sens. 60, 323–338. https://doi.org/10.1016/j.isprsjprs.2006.05.002.

Immitzer, M., Atzberger, C., Koukal, T., 2012. Tree Species Classification with Random Forest Using Very High Spatial Resolution 8-Band WorldView-2 Satellite Data. Remote Sens. 4, 2661–2693. https://doi.org/10.3390/rs4092661.

Immitzer, M., Neuwirth, M., Böck, S., Brenner, H., Vuolo, F., Atzberger, C., 2019. Optimal Input Features for Tree Species Classification in Central Europe Based on Multi-Temporal Sentinel-2 Data. Remote Sens. 11, 2599. https://doi.org/10.3390/rs11222599.

Ke, Y., Quackenbush, L.J., Im, J., 2010. Synergistic use of QuickBird multispectral imagery and LIDAR data for object-based forest species classification. Remote Sens. Environ. 114, 1141–1154. https://doi.org/10.1016/j.rse.2010.01.002.

Koenig, K., Höfle, B., 2016. Full-Waveform Airborne Laser Scanning in Vegetation Studies—A Review of Point Cloud and Waveform Features for Tree Species Classification. Forests 7, 198. https://doi.org/10.3390/f7090198.

Kraus, K., Pfeifer, N., 1998. Determination of terrain models in wooded areas with airborne laser scanner data. ISPRS J. Photogramm. Remote Sens. 53, 193–203. https://doi.org/10.1016/S0924-2716(98)00009-4.

RIEGL Laser Measurement Systems, 2010. Riegl Data Sheet LMS-Q560 [WWW Document]. URL http://www.riegl. com/uploads/tx_pxpriegldownloads/10_DataSheet_Q560_20-09 -2010_01.pdf (accessed 17.2.22).

RIEGL Laser Measurement Systems, 2012. Riegl Data Sheet LMS-Q680i [WWW Document]. URL http://www.riegl. com/uploads/tx_pxpriegldownloads/10_DataSheet_LMS-Q680i _28-09-2012_01.pdf (accessed 17.2.22).

Lawrence, R.L., Wood, S.D., Sheley, R.L., 2006. Mapping invasive plants using hyperspectral imagery and Breiman Cutler classifications (randomForest). Remote Sens. Environ. 100, 356–362. https://doi.org/10.1016/j.rse.2005.10.014.

Le Dez, M., Robin, M., Launeau, P., 2021. Contribution of Sentinel-2 satellite images for habitat mapping of the Natura 2000 site 'Estuaire de la Loire' (France). Remote Sens. Appl. Soc. Environ. 24, 100637 https://doi.org/10.1016/j.rsase.2021.100637.

Lechner, M., Dostálová, A., Hollaus, M., Atzberger, C., Immitzer, M., 2022. Combination of Sentinel-1 and Sentinel-2 Data for Tree Species Classification in a Central European Biosphere Reserve. Remote Sens. 14, 2687. https://doi.org/10.3390/rs14112687.

Leiterer, R., Torabzadeh, H., Furrer, R., Schaepman, M.E., Morsdorf, F., 2015. Towards Automated Characterization of Canopy Layering in Mixed Temperate Forests Using Airborne Laser Scanning. Forests 6, 4146–4167. https://doi.org/10.3390/f6114146.

Li, N., Liu, C., Pfeifer, N., 2019. Improving LiDAR classification accuracy by contextual label smoothing in post-processing. ISPRS J. Photogramm. Remote Sens. 148, 13–31. https://doi.org/10.1016/j.isprsjprs.2018.11.022.

Liaw, A., Wiener, M., 2002. Classification and Regression by randomForest. R News 2, 18–22.

Lindberg, E., Olofsson, K., Holmgren, J., Olsson, H., 2012. Estimation of 3D vegetation structure from waveform and discrete return airborne laser scanning data. Remote Sens. Environ. 118, 151–161. https://doi.org/10.1016/j.rse.2011.11.015.

McElwee, P., 2021. Climate Change and Biodiversity Loss: Two Sides of the Same Coin. Curr. Hist. 120, 295–300. https://doi.org/10.1525/curh.2021.120.829.295.

Meyer, H., Reudenbach, C., Hengl, T., Katurji, M., Nauss, T., 2018. Improving performance of spatio-temporal machine learning models using forward feature selection and target-oriented validation. Environ. Model. Softw. 101, 1–9. https://doi.org/10.1016/j.envsoft.2017.12.001.

Morsdorf, F., Kötz, B., Meier, E., Itten, K.I., Allgöwer, B., 2006. Estimation of LAI and fractional cover from small footprint airborne laser scanning data based on gap fraction. Remote Sens. Environ. 104, 50–61. https://doi.org/10.1016/j.rse.2006.04.019.

Nijland, W., Coops, N.C., Nielsen, S.E., Stenhouse, G., 2015. Integrating optical satellite data and airborne laser scanning in habitat classification for wildlife management. Int. J. Appl. Earth Obs. Geoinformation 38, 242–250. https://doi.org/10.1016/j.jag.2014.12.004.

Onojeghuo, A.O., Onojeghuo, A.R., Cotton, M., Potter, J., Jones, B., 2021. Wetland mapping with multi-temporal sentinel-1 & -2 imagery (2017–2020) and LiDAR data in the grassland natural region of alberta. GIScience Remote Sens. 58, 999–1021. https://doi.org/10.1080/15481603.2021.1952541.

OPALS Development Team, 2022. OPALS - Orientation and Processing of Airborne Laser Scanning data [WWW Document]. URL https://opals.geo.tuwien.ac.at/html/stable/index.html (accessed 18.5.22).

Osińska-Skotak, K., Radecka, A., Ostrowski, W., Michalska-Hejduk, D., Charyton, J., Bakuła, K., Piórkowski, H., 2021. The Methodology for Identifying Secondary Succession in Non-Forest Natura 2000 Habitats Using Multi-Source Airborne Remote Sensing Data. Remote Sens. 13, 2803. https://doi.org/10.3390/rs13142803.

Pesaresi, S., Mancini, A., Quattrini, G., Casavecchia, S., 2020. Mapping Mediterranean Forest Plant Associations and Habitats with Functional Principal Component Analysis Using Landsat 8 NDVI Time Series. Remote Sens. 12, 1132. https://doi.org/10.3390/rs12071132.

Pesaresi, S., Mancini, A., Quattrini, G., Casavecchia, S., 2022. Functional Analysis for Habitat Mapping in a Special Area of Conservation Using Sentinel-2 Time-Series Data. Remote Sens. 14, 1179. https://doi.org/10.3390/rs14051179.

Pfeil, I., Reuß, F., Vreugdenhil, M., Navacchi, C., Wagner, W., 2020. Classification of Wheat and Barley Fields Using Sentinel-1 Backscatter, in: IGARSS 2020 - 2020 IEEE International Geoscience and Remote Sensing Symposium. Presented at the IGARSS 2020 - 2020 IEEE International Geoscience and Remote Sensing Symposium, pp. 140–143. 10.1109/IGARSS39084.2020.9323560.

Plakman, V., Janssen, T., Brouwer, N., Veraverbeke, S., 2020. Mapping Species at an Individual-Tree Scale in a Temperate Forest, Using Sentinel-2 Images, Airborne Laser Scanning Data, and Random Forest Classification. Remote Sens. 12, 3710. https://doi.org/10.3390/rs12223710.

Puliti, S., Gobakken, T., Ørka, H.O., Næsset, E., 2017. Assessing 3D point clouds from aerial photographs for species-specific forest inventories. Scand. J. For. Res. 32, 68–79. https://doi.org/10.1080/02827581.2016.1186727.

QGIS Development Team, 2022. QGIS Geographic Informatino System. Open Source Geospatial Foundation Project. [WWW Document]. URL http://qgis.osgeo.org (accessed 18.5.22).

R Development Core Team, 2022. The R Project for Statistical Computing [WWW Document]. URL https://www.r-project.org/ (accessed 18.5.22).

Räsänen, A., Kuitunen, M., Tomppo, E., Lensu, A., 2014. Coupling high-resolution satellite imagery with ALS-based canopy height model and digital elevation model in object-based boreal forest habitat type classification. ISPRS J. Photogramm. Remote Sens. 94, 169–182. https://doi.org/10.1016/j.isprsjprs.2014.05.003.

Rouault, E., Warmerdam, F., Schwehr, K., Kiselev, A., Butler, H., Łoskot, M., Szekeres, T., Tourigny, E., Landa, M., Miara, I., Elliston, B., Kumar, C., Plesea, L., Morissette, D., Jolma, A., Dawson, N., 2022. GDAL. https://doi.org/10.5281/ZENODO.5884351.

Schindler, K., 2012. An Overview and Comparison of Smooth Labeling Methods for Land-Cover Classification. IEEE Trans. Geosci. Remote Sens. 50, 4534–4545. https://doi.org/10.1109/TGRS.2012.2192741.

Sheeren, D., Fauvel, M., Josipović, V., Lopes, M., Planque, C., Willm, J., Dejoux, J.-F., 2016. Tree Species Classification in Temperate Forests Using Formosat-2 Satellite Image Time Series. Remote Sens. 8, 734. https://doi.org/10.3390/rs8090734.

Sittaro, F., Hutengs, C., Semella, S., Vohland, M., 2022. A Machine Learning Framework for the Classification of Natura 2000 Habitat Types at Large Spatial Scales Using MODIS Surface Reflectance Data. Remote Sens. 14, 823. https://doi.org/10.3390/rs14040823.

Skidmore, A.K., Coops, N.C., Neinavaz, E., Ali, A., Schaepman, M.E., Paganini, M., Kissling, W.D., Vihervaara, P., Darvishzadeh, R., Feilhauer, H., Fernandez, M., Fernández, N., Gorelick, N., Geijzendorffer, I., Heiden, U., Heurich, M., Hobern, D., Holzwarth, S., Muller-Karger, F.E., Van De Kerchove, R., Lausch, A., Leitão, P.J., Lock, M.C., Mücher, C.A., O'Connor, B., Rocchini, D., Roeoesli, C., Turner, W., Vis, J. K., Wang, T., Wegmann, M., Wingate, V., 2021. Priority list of biodiversity metrics to observe from space. Nat. Ecol. Evol. 5, 896–906. https://doi.org/10.1038/s41559-021-01451-x.

Sørensen, R., Zinko, U., Seibert, J., 2006. On the calculation of the topographic wetness index: evaluation of different methods based on field observations. Hydrol. Earth Syst. Sci. 10, 101–112. https://doi.org/10.5194/hess-10-101-2006.

Szporak-Wasilewska, S., Piórkowski, H., Ciężkowski, W., Jarzombkowski, F., Sławik, Ł., Kopeć, D., 2021. Mapping Alkaline Fens, Transition Mires and Quaking Bogs Using Airborne Hyperspectral and Laser Scanning Data. Remote Sens. 13, 1504. https://doi.org/10.3390/rs13081504.

Tarantino, C., Forte, L., Blonda, P., Vicario, S., Tomaselli, V., Beierkuhnlein, C., Adamo, M., 2021. Intra-Annual Sentinel-2 Time-Series Supporting Grassland Habitat Discrimination. Remote Sens. 13, 277. https://doi.org/10.3390/rs13020277.

Trimble, 2022. Trimble Inpho | Trimble Geospatial [WWW Document]. URL https://de.geospatial.trimble.com/products-and-solutions/trimble-inpho (accessed 25.5.22).

Umweltbundesamt, 2021. Schutzgebiete [WWW Document]. URL https://www.umweltbundesamt.at/umweltthemen/naturschutz/schutzgebiete (accessed 26.4.22).

van Ewijk, K.Y., Treitz, P.M., Scott, N.A., 2011. Characterizing Forest Succession in Central Ontario using Lidar-derived Indices. Photogramm. Eng. Remote Sens. 77, 261–269. https://doi.org/10.14358/PERS.77.3.261.

Vreugdenhil, M., Wagner, W., Bauer-Marschallinger, B., Pfeil, I., Teubner, I., Rüdiger, C., Strauss, P., 2018. Sensitivity of Sentinel-1 Backscatter to Vegetation Dynamics: An Austrian Case Study. Remote Sens. 10, 1396. https://doi.org/10.3390/rs10091396.

Vuolo, F., Neuwirth, M., Immitzer, M., Atzberger, C., Ng, W.-T., 2018. How much does multi-temporal Sentinel-2 data improve crop type classification? Int. J. Appl. Earth Obs. Geoinformation 72, 122–130. https://doi.org/10.1016/j.jag.2018.06.007.

Wagner, W., Hollaus, M., Briese, C., Ducic, V., 2008. 3D vegetation mapping using small-footprint full-waveform airborne laser scanners. Int. J. Remote Sens. 29, 1433–1452. https://doi.org/10.1080/01431160701736398.

Stadt Wien - https://data.wien.gv.at, 2020. Biotoptypenkartierung Wien - data.gv.at [WWW Document]. Biotoptypenkartierung Wien Sel. Flächige Kart. Leb. Biotope Gem Wien. Naturschutz-Verordn. Flora-Fauna-Habitat-Richtlin. FFH-RL Sowie Biotope Rote-Liste-Biotope Umweltbundesamtes UBA Auf Grundl. Phytotop-Kart. 1980er-Jahre. URL https://www.data.gv.at/katalog/dataset/stadt-wien_biotoptypenkartierungwien (accessed 17.2.22).

Zhong, L., Gong, P., Biging, G.S., 2014. Efficient corn and soybean mapping with temporal extendability: A multi-year experiment using Landsat imagery. Remote Sens. Environ. 140, 1–13. https://doi.org/10.1016/j.rse.2013.08.023.

Zlinszky, A., Schroiff, A., Kania, A., Deák, B., Mücke, W., Vári, Á., Székely, B., Pfeifer, N., 2014. Categorizing Grassland Vegetation with Full-Waveform Airborne Laser Scanning: A Feasibility Study for Detecting Natura 2000 Habitat Types. Remote Sens. 6, 8056–8087. https://doi.org/10.3390/rs6098056.

Zlinszky, A., Deák, B., Kania, A., Schroiff, A., Pfeifer, N., 2015. Mapping Natura 2000 Habitat Conservation Status in a Pannonic Salt Steppe with Airborne Laser Scanning. Remote Sens. 7, 2991–3019. https://doi.org/10.3390/rs70302991.